EAI Endorsed Transactions
on Sustainable Manufacturing and Renewable Energy Research Article EAI.EU

FEM-Based Analysis of Interference Fit for High-Precision Mechanical Assemblies

Truong Minh Nhat[1, 2, 3, *], Pham Manh Truong[3], Ngo Thanh Binh[4], Vo Hoang Khang[1, 2, 3], Huynh Phat Dat[1, 2] and Vo Tung Linh[3]

[1] Faculty of Mechanical Engineering, Ho Chi Minh City University of Technology (HCMUT), 268 Ly Thuong Kiet, District 10, Ho Chi Minh, Vietnam
[2] Vietnam National University-Ho Chi Minh City (VNU-HCM), Linh Trung Ward, Thu Duc City, Ho Chi Minh, Vietnam
[3] Cao Thang Technical College, 65 Huynh Thuc Khang Street, Ben Nghe Ward, District 1, Ho Chi Minh City
[4] Southern Branch of Joint Vietnam-Russia Tropical Science and Technology Research Center, 3/2 Street, Ward 10, District 10, Ho Chi Minh City

Abstract

This study presents an interference fit study that supports the design and evaluation of press-fit assemblies. The simulation model is based on the Thick-Walled Cylinder Theory (TCT) to accurately predict contact pressure, pressing force, and stress distribution during assembly and disassembly. The shaft-bearing assembly is machined with high precision for experimentation. The results show good agreement between the FEM simulation and the theoretical stress distribution, confirming the mechanical behavior of the interference fit. Experimental verification of the pressing force is also performed and compared with the simulation, showing consistent trends. The simulation model helps evaluate the assembly performance in different tolerance and coefficient of friction domains, providing a practical solution for high-precision mechanical assemblies.

Keywords: interference fit, thick-walled cylinder theory, Finite Element Method.

Received on 27 April 2025, accepted on 15 June 2025, published 05 August 2025

doi: 10.4108/eetsmre.9179

1. Introduction

Interference fit (also known as press fit) is one of the popular methods in the field of mechanical assembly, especially for connecting two parts with equal nominal dimensions. When the intermediate or press-fit joint is used, the resistance force is generated due to the interference between the contact surfaces [1, 2]. This assembly method is widely used in assemblies that require high precision in tolerances and structural rigidity, such as shafts–gears or shafts–bearings. By avoiding the use of threaded or bolted joints, interference fit reduces the risk of damage due to vibration while enhancing the load-bearing and torque-transmission capabilities in various industrial applications [2, 3].

To calculate and design interference fit, important factors such as geometric deviations (roundness, cylindricity), surface roughness, tolerance design and material properties significantly influence to the press-fit force and resistance force of the assembly [1, 4, 5]. Many studies have proposed analytical methods to predict the press-fit curve or determine the contact pressure distribution. Of these studies, Wang et al.[2] introduced a new calculation method to predict the press-fit curve according to different interference levels. The overlap fitting process was simulated using ANSYS Workbench to analyze the influence of the non-contact area on the press-fit force. In addition, Arun P. Raj et al. [5] investigated the combined effects of roundness, cylindricity and roughness surface on the axial load capacity of interference fits. A linear regression model was proposed to predict axial load based on interference, cylindricity and roughness surface.

* Corresponding author. Email: truongminhnhat@caothang.edu.vn

Many new methods have also been proposed to improve and optimize the design. Y. Zhang et al. [1] applied the selective assembly method to increase the accuracy and meet the requirements of reducing production costs. The tolerance method using I_{max} and I_{min} curves was developed to provide a guideline for interference fit design. Guillaume Biron et al. [6] proposed a method to optimize the design of interference fit under fatigue load using the Sequential Approximate Multi-Objective Optimization algorithm (SAMOO). Niels L. Pedersen [7] introduced methods to optimize the design of interference fit between shaft and hub by improving the contact pressure distribution. Therefore, it helps reduce the risk of damage by fretting fatigue failure. This approach enhances the service life of interference fit by limiting fretting fatigue. Elvio Bonisoli et al. [8] developed a meta-model based on Polynomial Chaos Expansion (PCE) to estimate the overlap and assembly force, combined with Experimental Modal Analysis (EMA). This model was applied to a real case in the automotive industry, specifically the double joint of steel wheels of vehicles. Xingyuan Wang et al. [9] built a theoretical model, simulated FEM using ANSYS and experimented on different material pairs (Ni36CrTiAl – 50Ni-50Fe, AISI 1045 – AISI 1045). The results were compared with the simulation under full contact conditions.

In addition to analytical models, the Finite Element Method (FEM) has become an effective design tool for simulating the stresses, strains, and friction forces generated in the contact zone [1, 10]. Using FEM, complex geometric elements and variable boundary conditions can be analyzed in more detail, thereby optimizing tolerance parameters and press-fitting processes [11]. Moreover, the integration of “selective assembly” processes, based on size and tolerance grouping, helps to limit cumulative deviations, improve assembly quality, and reduce manufacturing costs [3].

However, geometric structures, technological processes, and fluctuations in friction properties can vary greatly in practice. Manual calculations or table lookups still do not meet the automation needs in modern industrial environments. Therefore, the development of an “Interference Fit Calculator” program that automatically calculates design parameters and checks assembly tolerances is of particular interest. This calculator will allow designers to quickly evaluate mounting forces, resistance forces and surface deformations during the press-fit process, while integrating FEM models and analytical methods to widely simulate assembly scenarios.

Based on the requirements, this study aims to develop a set of computational tools to support interference fit design. The tool integrates analytical models to help predict mounting force and resistance force based on tolerance parameters, surface roughness and geometric accuracy of the mounting performance. The next section will present the theoretical basis and typical results, helping to complete the systematic interference fit design method.

2. Methodology

2.1. Geometric model

To study the behavior of common joints in engineering, the model system is built according to the modularization principle, Figure 1A. Specifically, multiple disassembly modules were designed, each module represents a group of typical joints commonly encountered in practice such as spline joints, threaded joints, conical joints, smooth joints with tolerances, and especially roller bearing joints.

Among the designed models, the roller bearing joint model is selected for the simulation model (Figure 1B) because this is a classic model, a popular and highly accurate joint. In addition, the shaft and bearing joint when disassembling and assembling requires control of the applied force, checking the assembly tolerance, heating or cold pressing techniques. Roller bearing joints are often under high loads and high speeds, so any deviation in operation and applied force when disassembling and assembling can damage the parts, affecting the working accuracy of the entire machine system.

(A)

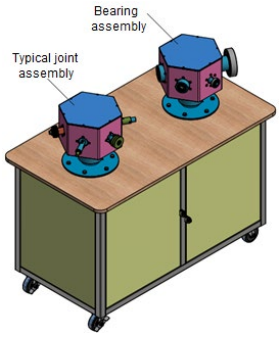

(B)

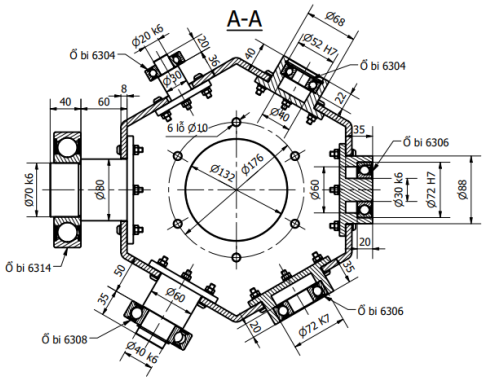

Figure 1. Design model; (A) Overall model and (B) Assembly drawing of the bearing assembly.

In the experiment, the bearing is installed by heating method to avoid changing the condition of the mounting surface, reducing the error for the bearing pressing test, Figure 1A. The process of removing the shaft from the bearing was performed using an Instron SATEC Model

2294-5V hydraulic universal testing machine with a maximum pressing force of 200 tons, Figure 1B. The test specimen was placed concentrically with the pressing shaft to ensure even force application and avoid deviation during the process. The test was conducted with a loading rate of 10 mm/min.

(A)

(B)

Figure 2. (A) Assembly of bearing by heating method and (B) Hydraulic press bearing removal.

2.2. Model simulation

In this simulation, the contact stress zones and contact pressures generated from mounting the 6314 bearing onto the shaft are primarily illustrated in Figure 3. The simulation is conducted under completely ideal conditions, assuming no geometric deviations and positional tolerance. The interference allowance is set to 0.16 mm and the coefficient of friction is set to 0.6. The mechanical properties of the materials are shown in Table 1.

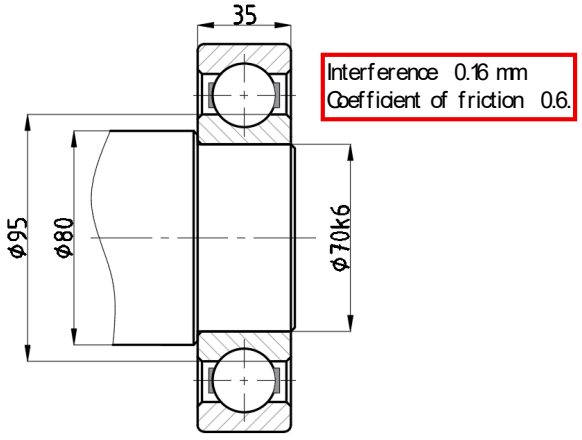

Figure 3. Bearing model used for design in simulation.

Table 1. Shaft material properties.

Name	Value	Unit	Property group
Young'modulus	2.1E11	Pa	Basic
Poisson's ratio	0.3	1	Basic
Density	7800	Kg/m^3	Basic

2.3. Theoretical assumptions

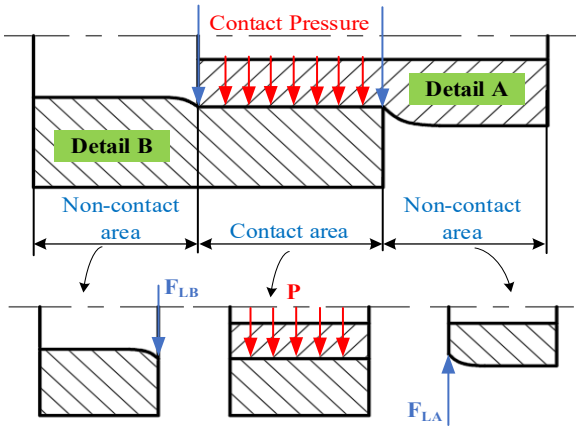

Figure 4. Physical model of force action.

The force generated during assembly consists of two components: (1) the pressure acting on the tube wall, which is analyzed by thick-walled cylinder theory (TCT)) and (2) resistance at non-contact areas, Figure 4.

Force acting on the tube wall

The contact pressure is P, the outer radius decrease of part A is u_1, and the inner radius increase of part B is u_2 (Figure 5), u_1 and u_2 can be calculated by TCT: [12]

$$u_1 = \frac{\mathrm{Pr}_2}{E_1}\left(\frac{r_1^2 + r_2^2}{r_2^2 - r_1^2} + \mu_1\right) \quad (1)$$

$$u_2 = \frac{\mathrm{Pr}_2}{E_2}\left(\frac{r_3^2 + r_2^2}{r_3^2 - r_2^2} + \mu_2\right) \quad (2)$$

Where r_1 is the inner radius of part A; r_2 is the contact radius; r_3 is the outer radius of part B; E_1 is the elastic modulus of part A; μ_1 is the Poisson's ratio of part A; E_2 is the elastic modulus of part B and μ_2 is the Poisson's ratio of part B.

The outer radius of part A is larger than the inner radius of part B by an amount of Z.

$$Z = u_1 + u_2 \quad (3)$$

Substituting equations (1) and (2) into equation (3), obtain the contact pressure.

$$P = \frac{Z}{\frac{r_2}{E_1}\left(\frac{r_1^2+r_2^2}{r_2^2-r_1^2}+\mu_1\right)+\frac{r_2}{E_2}\left(\frac{r_3^2+r_2^2}{r_3^2-r_2^2}+\mu_2\right)} \quad (4)$$

The frictional force generated by the contact area can be calculated based on Coulomb's law of friction:

$$F_f = 2\pi r_2 LPf \quad (5)$$

Where f is the coefficient of friction and L is the contact length.

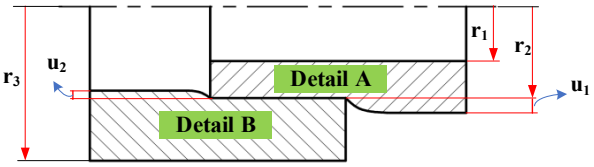

Figure 5. Dimensions of the assembled part.

Resistance in non-contact areas

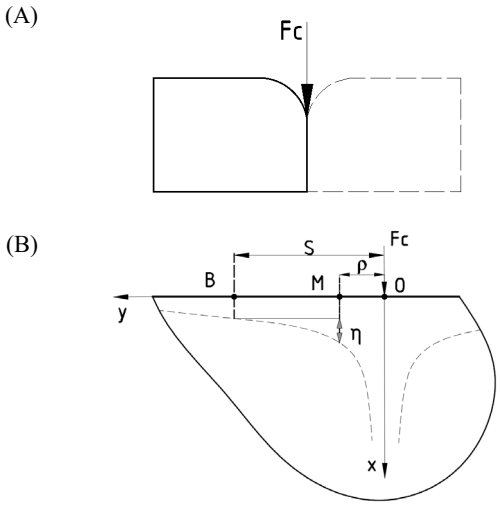

Figure 6. Simplified model for resistant force.

TCT cannot accurately predict the compressive force because it ignores the resistance created by the non-contact regions. Therefore, to establish an analytical method, it is necessary to derive a method for calculating the resistance force. Consider a force acting on a plate of large length and certain thickness, Figure 6A. [2]

According to Figure 6B, the y-coordinates of points B and M are s and ρ, respectively. Point B is defined as the reference point. So the relative deformation between B and M in the vertical direction can be determined.

$$\eta = \frac{2F_c\left(1-\mu^2\right)}{\pi E}\ln\frac{s}{\rho} \quad (6)$$

$$\rho_{\min} = s \times \exp\left(-\frac{\pi E\eta}{2F_c\left(1-\mu^2\right)}\right) \quad (7)$$

The concentrated force generated by the non-contact region between part A and part B can be calculated using the following equations.

$$F_{LA} = \frac{1}{2}F_c = \frac{\pi\eta_A E_1}{4\left(1-\mu_1^2\right)\ln\frac{s_A}{\rho_{\min\_A}}} \quad (8)$$

$$F_{LB} = \frac{1}{2}F_c = \frac{\pi\eta_B E_2}{4\left(1-\mu_2^2\right)\ln\frac{s_B}{\rho_{\min\_B}}} \quad (9)$$

Therefore the drag force can be calculated by equations (8) and (9).

$$F_r = 2\pi r_2 f\left(F_{LA}+F_{LB}\right) \quad (10)$$

Finally, the pressing force can be calculated according to equations (5) and (10).

$$F = F_f + F_r \quad (11)$$

3. Results and discussion

3.1 Distribution stress

Figure 7 illustrates the von Mises stress distribution in the mounting area between the bearing and the shaft. The maximum stress occurs at the shaft shoulder, where stress concentration typically appears. The maximum von Mises stress is about 16×10^2 (MPa), which remains below the yield strength of standard bearing steels (e.g, AISI 52100). This stress distribution is still within the elastic deformation range, ensuring safe press fitting under certain conditions.

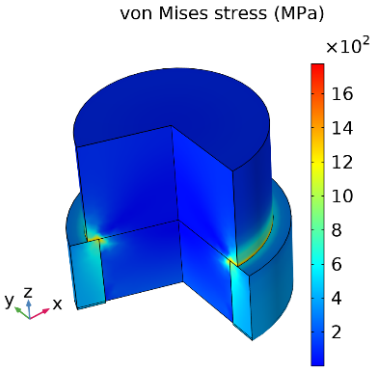

Figure 7. Distribution of von Mises stress after press-fitting the bearing onto the shaft.

The von Mises stress distribution in the radial direction shows good agreement with the TCT theory, as illustrated in Figure 8 and Figure 9. The stress distribution reflects the force transmission mechanism of the interference joint.

Specifically, the stress increases from the center of the shaft towards the contact surface of the two parts (0.035 m), then gradually decreases across the outer ring of the bearing. This confirms the location of the maximum contact pressure and demonstrates the consistency of the simulation with the analytical models.

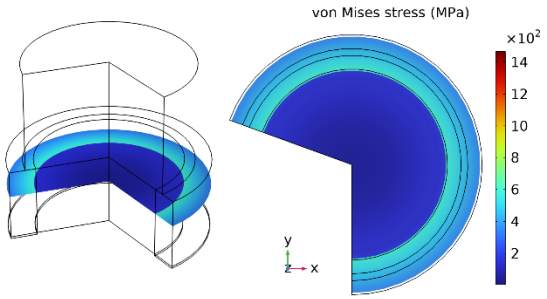

Figure 8. Distribution of von Mises stress at cross-sectional of the press-fit assembly.

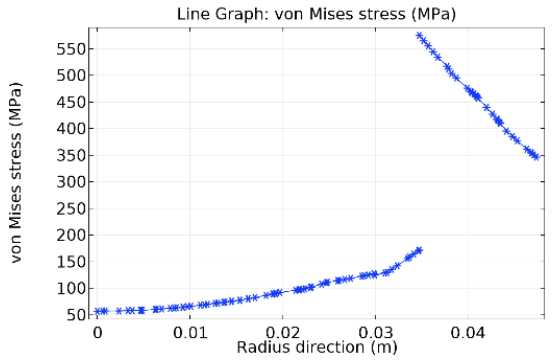

Figure 9. Distribution of von Mises stress in the radial direction at a position 20 mm from the shaft end.

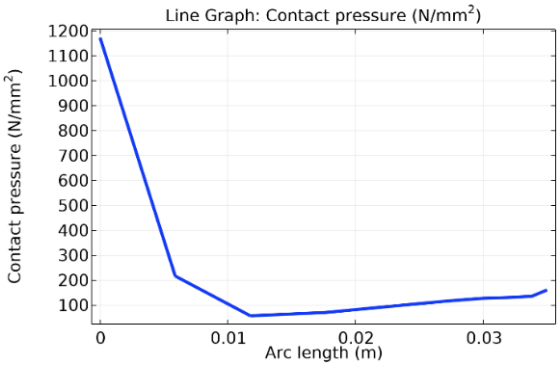

Figure 10. Contact pressure along the contact surface (position 0 m is shoulder; position 0.035 m is end face).

Figure 10 illustrates the distribution of contact pressure (N/mm²) along the axial length of the shaft-bearing joint. The contact pressure reaches the max value at the shaft shoulder of about 1200 N/mm². After that, the pressure drops sharply to a lower level and stable at about 100 to 200 (N/mm²). Stress concentration occurs at the shoulder of the shaft, which is susceptible to local plastic deformation, fatigue cracking or misalignment if the design is not reasonable.

3.2 Compression force

In this model, Equation (12) is used to calculate the pressing force required when removing the bearing from the shaft, as follows:

$$F = 2\pi rf \int_0^l Pdz \tag{12}$$

Where f is the friction coefficient, P is the contact pressure, r is the radius of shaft, and z is an axial coordinate along the contact region.

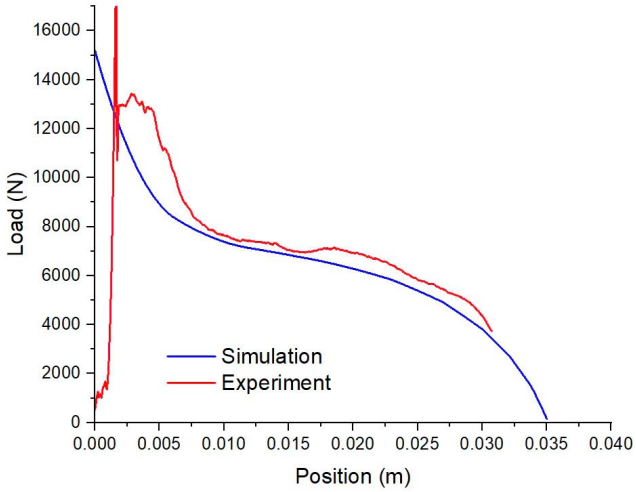

Figure 11. Graph of compressive force results between simulation and experiment.

Figure 11 illustrates the compressive force required to press the bearing off the shaft. The horizontal axis represents the displacement (position) of the pressing-fit remove process, while the vertical axis shows the applied load (N). The graph (Figure 11) shows the experimental result value of 3 test specimens which is the average value with the same size and tolerance parameters.

In the early stage (0 – 0.0025 m), the experimental curve increases rapidly from the beginning, reaching nearly 16,000 N, which is significantly higher than the simulation. This discrepancy may be attributed to initial misalignment, surface roughness, or micro-geometrical deviations that are not considered in the simulation. In the intermediate stage (0.0025 – 0.030 m), both curves have similar trends with decreasing loads, indicating the relative stability of the

contact interface. However, the experimental load is still higher than the simulation, which may be due to the stick-slip behavior when sliding at low speeds. In the final stage (0.030 – 0.035 m), the curves converge towards the end, indicating that both the simulation and experimental models agree on the final assembly behavior. This convergence supports the validity and reliability of the simulation in capturing the overall mechanical response of the interference joint.

Conclusion

This study developed and validated an “Interference Fit” that integrates FEM analysis and simulation models to support the design and evaluation of press-fit mechanical assemblies. Through analysis of the bearing interference fit, the simulation results show good agreement with the theoretical stress distribution based on TCT theory.

- The FEM analysis shows that the maximum von Mises stress occurs at the shaft shoulder, which matches the expected stress concentration region.

- Experimental verification of the press-out force also - validates the simulation results, with both curves showing consistent trends across all displacement stages. The small differences in the peak load are attributed to geometrical defects, surface roughness, and stick-slip effects during slow disassembly.

The developed tool enables designers to predict the press-in force, contact stress, and deformation behavior with high confidence, especially for high-precision mechanical assemblies.

Acknowledgements

We would like to express our sincere gratitude to the Faculty of Mechanical Engineering, Cao Thang Technical College, for their support and facilitation in the fabrication of the equipment used in this research. The valuable assistance from the faculty members and the provided facilities played a crucial role in the success of this study.

References

[1] Y. Zhang, B. McClain, and X. J. I. J. o. M. S. Fang, "Design of interference fits via finite element method," vol. 42, no. 9, pp. 1835-1850, 2000.

[2] X. Wang, Z. Lou, X. Wang, and C. J. J. o. M. P. T. Xu, "A new analytical method for press-fit curve prediction of interference fitting parts," vol. 250, pp. 16-24, 2017.

[3] G. Marcuccio, E. Bonisoli, S. Tornincasa, J. E. Mottershead, E. Patelli, and W. J. T. J. o. S. A. f. E. D. Wang, "Image decomposition and uncertainty quantification for the assessment of manufacturing tolerances in stress analysis," vol. 49, no. 8, pp. 618-631, 2014.

[4] G.-M. Yang, J. C. Coquille, J. F. Fontaine, M. J. I. j. o. S. Lambertin, and Structures, "Influence of roughness on characteristics of tight interference fit of a shaft and a hub," vol. 38, no. 42-43, pp. 7691-7701, 2001.

[5] A. P. Raj, A. Bhatti, and P. J. P. o. t. I. o. M. E. Dhanish, Part J: Journal of Engineering Tribology, "Combined effect of cylindricity, roundness and roughness on axial load-carrying ability of interference fits," vol. 234, no. 11, pp. 1697-1711, 2020.

[6] G. Biron, A. Vadean, L. J. S. Tudose, and m. optimization, "Optimal design of interference fit assemblies subjected to fatigue loads: A sequential approximate multi-objective optimization approach," vol. 47, pp. 441-451, 2013.

[7] N. L. J. S. Pedersen and m. optimization, "On optimization of interference fit assembly," vol. 54, pp. 349-359, 2016.

[8] E. Bonisoli, G. Marcuccio, S. J. M. S. Venturini, and S. Processing, "Interference fit estimation through stress-stiffening effect on dynamics," vol. 160, p. 107919, 2021.

[9] X. Wang, Z. Lou, X. Wang, X. Hao, and Y. J. P. o. t. I. o. M. E. Wang, Part C: Journal of Mechanical Engineering Science, "Prediction of stress distribution in press-fit process of interference fit with a new theoretical model," vol. 233, no. 8, pp. 2834-2846, 2019.

[10] F. Lanoue, A. Vadean, B. J. S. M. P. Sanschagrin, and Theory, "Finite element analysis and contact modelling considerations of interference fits for fretting fatigue strength calculations," vol. 17, no. 10, pp. 1587-1602, 2009.

[11] H. Boutoutaou, M. Bouaziz, and J.-F. J. I. j. o. m. s. Fontaine, "Modelling of interference fits with taking into account surfaces roughness with homogenization technique," vol. 69, pp. 21-31, 2013.

[12] S. P. Timoshenko and J. M. Gere, *Theory of elastic stability*. Courier Corporation, 2009.